Research Article

Cancer Immunology Research

All-Trans Retinoic Acid Prevents Osteosarcoma Metastasis by Inhibiting M2 Polarization of Tumor-Associated Macrophages

Qian Zhou, Miao Xian, Senfeng Xiang, Danyan Xiang, Xuejing Shao, Jincheng Wang, Ji Cao, Xiaochun Yang, Bo Yang, Meidan Ying, and Qiaojun He

Abstract

M2-polarized tumor-associated macrophages (TAM) play a critical role in cancer invasion and metastasis. Here, we report that M2 macrophages enhanced metastasis of K7M2 WT osteosarcoma cells to the lungs in mice, thus establishing M2 TAMs as a therapeutic target for blocking osteosarcoma metastasis. We found that *all-trans* retinoic acid (ATRA) inhibited osteosarcoma metastasis via inhibiting the M2 polarization of TAMs. ATRA suppressed IL13- or IL4-induced M2-type macrophages, and then inhibited migration of osteosarcoma cells as promoted by M2-type macrophages *in vitro*. ATRA reduced the number of pulmonary metastatic nodes of osteosarcoma and decreased expression of M2-type macrophages in metastatic nodes both in intravenous injection and orthotopic transplantation models. ATRA's effect was independent of conventional STAT3/6 or C/EBPβ signaling, which regulate M2-like polarization of macrophages. Quantitative genomic and functional analyses revealed that MMP12, a macrophage-secreted elastase, was elevated in IL13-skewed TAM polarization, whereas ATRA treatment downregulated IL13-induced secretion of MMP12. This downregulation correlates with the antimetastasis effect of ATRA. Our results show the role of TAM polarization in osteosarcoma metastasis, identify a therapeutic opportunity for antimetastasis treatment, and indicate ATRA treatment as an approach for preventing osteosarcoma metastasis via M2-type polarization intervention. *Cancer Immunol Res; 5(7); 547–59. ©2017 AACR.*

Introduction

Osteosarcoma accounts for 60% of all malignant childhood bone tumors (1). With combined treatment (neoadjuvant chemotherapy, surgery, and adjuvant chemotherapy), the 5-year survival rate of patients with no metastatic disease at diagnosis is 60% to 70% (2); for patients who present with metastasis, the chance of survival drops to less than 30% (3). Treatment-refractory pulmonary metastasis is the major complication of osteosarcoma.

Microenvironment determines tumor progression and metastasis (4). The presence and density of tumor-associated macrophages (TAM) correlates with tumor cell proliferation, invasion, metastasis, and poor prognosis (5, 6). TAMs comprise up to 50% of the total tumor volume and predominantly display an M2 (alternatively activated) phenotype (7). M2-type TAMs are key drivers of tumors behavior, affecting tumor progression and metastasis. In many cancers, including breast (8), prostate (9), colon (10), and stomach (11), M2 TAMs contribute to neoplastic metastasis by stimulating inflammation, angiogenesis, invasion, intravasation, and tissue remodeling (5, 12, 13). Clinical studies show that osteosarcoma tumors were infiltrated with a heterogeneous population of TAMs, including both M1 (classically activated) and M2 phenotypes. In osteosarcoma, the constitutive presence of M1 macrophages may have an antimetastatic rather than a prometastatic effect (14).

Here, we investigated the metastatic effect of M2-type macrophages in osteosarcoma. Our data showed that M2-type macrophages promote pulmonary metastasis of osteosarcoma. We conclude that TAMs, especially M2 TAMs, may be a therapeutic target for blocking osteosarcoma metastasis.

To identify a regulatory molecule, we studied all-trans retinoic acid (ATRA), the active derivation of vitamin A, which regulates polarization of macrophages. ATRA induces cellular differentiation and arrests proliferation of tumor cells (15, 16). ATRA activates transcription factors such as STATs, C/EBPβ, which regulate TAM polarization in cancer cells (17–19). ATRA also inhibits the invasion of human breast cancer cells and gastric cancer cells (20–22). Although ATRA affects tumor-promoting abilities of TAM (23), its role in educating TAM remains unclear. Here, we studied the effect of ATRA on metastasis of osteosarcoma cells.

We determined that M2-like macrophages could promote pulmonary metastasis of osteosarcoma, and ATRA effectively skewed macrophages away from M2 polarization induced by IL13 and IL4. We also found that ATRA prevents migration of osteosarcoma cells both *in vitro* and *in vivo*. Thus, ATRA may be useful as an antimetastatic agent functioning to block M2 polarization of TAMs.

Zhejiang Province Key Laboratory of Anti-Cancer Drug Research, College of Pharmaceutical Sciences, Zhejiang University, Hangzhou, China.

Note: Supplementary data for this article are available at Cancer Immunology Research Online (http://cancerimmunolres.aacrjournals.org/).

Q. Zhou and M. Xian contributed equally to this article.

Corrected online January 8, 2020.

Corresponding Authors: Qiaojun He, Room 113, Institute of Pharmacology and Toxicology, College of Pharmaceutical Sciences, Zhejiang University, Hangzhou 310058, China. Phone/Fax: 86-571-88208400; E-mail: qiaojunhe@zju.edu.cn; and Meidan Ying, Room 427, Institute of Pharmacology and Toxicology, College of Pharmaceutical Sciences, Zhejiang University, Hangzhou 310058, China. Phone/Fax: 86-571-88208400; E-mail: mying@zju.edu.cn

doi: 10.1158/2326-6066.CIR-16-0259

Materials and Methods

Materials

Recombinant IL13 and IL4 were purchased from Peprotech, recombinant IFNγ was from R&D. LPS and ATRA was from Sigma. Clodronate Liposomes and PBS Liposomes were from clodronateliposomes.org. mmp408 was purchased from Merck.

Cell lines and cell culture

RAW264.7 cells and K7M2 WT (wild-type) cells were obtained from the Cell Bank of the China Science Academy (March 2013 and September 2013) and maintained in DMEM containing 10% FBS. Following receipt, cells were grown and frozen as a seed stock as they were available. Both cell lines were passaged for a maximum of 2 months, after which new seed stocks were thawed. Both of the cell lines were authenticated using DNA fingerprinting (variable number of tandem repeats), confirming that no cross-contamination occurred during this study. Cell lines were tested for mycoplasma contamination at least every month. Both of the cell lines were maintained at 37°C in a humidified atmosphere containing 5% CO_2.

Preparation of BMDM

Bone marrow isolation was performed as described previously (24). Bone marrow cells differentiated into bone marrow–derived macrophages (BMDM) with M-CSF (Cell Signaling Technology). After a 3-day incubation, BMDMs were rinsed with DMEM to remove nonadherent cells and then cultured with 10 ng/mL IL13 or IL4 for additional 5 days.

Preparation of K7M2 WT cell supernatant for RAW264.7 treatment

Once the K7M2 WT cells in 6-well culture plates had been cultured to 80% cell confluence, the DMEM medium was replaced with fresh medium with 2% serum and the cells were incubated for a further 24 hours followed by the harvesting of the supernatants from the cultures. Supernatant was centrifuged at 2,000 rpm to separate out the debris and stored at −80°C. RAW264.7 cells were treated with K7M2 WT supernatant to a final concentration of 50% (v/v) for 48 hours.

Conditioned medium preparation

Macrophage polarization was obtained by culturing cells with 20 ng/mL IL13 or IL4 for 48 hours. Where indicated, ATRA was added during macrophage polarization. Different polarized macrophages were incubated in serum free medium for 24 hours, after which culture supernatants were collected as conditioned medium (CM). CM was centrifuged at 2,000 rpm to separate out the debris and stored at −80°C. For stimulation with RAW264.7-CM (RM) or BMDM-CM (BM), K7M2 WT cells were supplemented with RM or BM to a final concentration of 50% (v/v).

Flow cytometry

Samples were incubated with PE-CD206, PE-CD86 (Biolegend), FITC-CD209 or FITC-F4/80 antibody (eBioscience) according to the manufacturer's instructions. For each sample, at least 1×10^4 cells should be analyzed.

Reverse transcription PCR

The quantitative real-time RT-PCR analysis was performed by TAKARA SYBR Premix EXTaqTM. The reaction mixtures containing SYBR Green were composed following the manufacturer's protocol. The sequences of the primers used for the quantitative RT-PCR were as follows: MRC1, forward: 5′-AGGGACCTGGATGGATGACA-3′; reverse: 5′-TGTACCGCACCCTCCATCTA-3′; PPAR-γ, forward: 5′-TTCGATCCGTAGAAGCCGTG-3′; reverse: 5′-TTGGCCCTCTGATGAGGA-3′; CCL3, forward: 5′-ACTGCCTGCTGCTTCTCCTACA-3′; reverse: 5′-AGGAAAATGACACCTGGCTGG-3′; CCL5, forward: 5′-CATATGGCTCGGACACCACTC-3′; reverse: 5′-CGACTGCAAGATTGGAGCAC-3′; MMP12, forward: 5′-TGGGCTTCTCTGCATCTGTG-3′; reverse: 5′-TTTGGTGACACGACGGAACA-3′; MMP14, forward: 5′-AGGCCAATGTTCGGAGGAAG-3′; reverse: 5′-TTCTCATGTCCCTCCCGGAT-3′; MMP13, forward: 5′-CAGCTATCCTGGCCACCTTC-3′; reverse: 5′-CAGGCACTCCACATCTTGGT-3′; MMP9, forward: 5′-AAACCCTGTGTTCCCGTT-3′; reverse: 5′-CAGGCTGTACCCTTGGTCTG-3′; ACTIN, forward: 5′-GGTCATCACTATTGGCAACG-3′; reverse: 5′-ACGGATGTCAACGTCACACT-3′. β-Actin was used as an internal control.

Matrigel invasion assay

Invasion assay was performed using membranes coated with Matrigel matrix (BD Science). Cell suspension (2×10^4 cells/mL) was placed in the top chamber with 0.2 mL different CM. For antibody neutralization invasion assay, antibodies to MMP9 and MMP12 (EIAab, Wuhan Eiaab Science Co., Ltd) were added in the CM to a final concentration of 2 μg/mL. After 24-hour incubation at 37°C, invaded cells were fixed with 100% MeOH and then stained with crystal violet. The stained cells were subsequently photographed and quantified.

Wound-healing assay

K7M2 WT cells were seeded in 24-well plates and cultured until they became 70% to 80% confluent. A pipette tip was used to make a straight scratch, and an artificial wound was formed. Image acquisition of wound fields was done. After different CM treatment for 24 hours, wound closure documentation was done with a phase-contrast microscope (Leica DMI4000B; Leica Microsystems). Image analysis was conducted with Adobe Photoshop CS5 software.

Immunofluorescence

Cryostat sections were fixed and permeated. F4/80, CD209, and CD86 antibodies were used, followed by Alexa Fluor 488 or 594. Nuclei were visualized by staining DAPI. F4/80-positive cells were quantitated by ImageJ software.

Immunohistochemistry (DAB)

Paraffin-embedded tissue sections were dewaxed, rehydrated, and subjected to microwave with PH 9.0 Tris-EDTA buffer for F4/80, CD209 and CD86 staining. Then Histostain-Plus Kit was used by following the manufacturer's instructions. The protein expression levels of F4/80, CD209, and MMP12 were expressed as the mean integrated optical density (IOD), a parameter describing the total amount of antibody labeling in the section using ImageJ software. The IOD was $\log_{10}$ transformed.

cDNA microarray

The RNA samples of were hybridized using Agilent Mouse Genome 4*44K Oligonucleotide Microarrays in the Shanghai Biotechnology Corporation. After scanning, hybridization signals were collected for further analysis. The entire microarray dataset is

available at the Gene Expression Omnibus database under accession no. GSE73564.

In vivo experimental metastasis assay

Four- to five-week-old female balb/c mice (National Rodent Laboratory Animal Resource, Shanghai, China) were used for all experiments. All animal experiments were carried out in accordance with the Institutional Animal Use and Care Committee. After the mice were euthanized, all lungs were dissected and then fixed with formalin. Tissue sections were stained with hematoxylin/eosin.

Coinoculated tumor model. K7M2 WT cells (1×10^6) mixed with or without CM (1:3) were injected into the tail vein of mice for 10 days. The weights of the mice were recorded until the animals were euthanized.

In vivo *pulmonary metastases animal study.* The mice were randomly assigned to four groups: control, ATRA-treatment, Clodronate liposomes-treatment and ATRA combined with Clodronate liposomes treatment groups. Mice were daily pretreated with 20 mg/kg ATRA (i.g.) or 200 μL Clodronate liposomes (i.p.) for 7 days before K7M2 WT cells injection. Balb/c mice were then injected with K7M2 WT cells: intravenous (1×10^6 cells) or intrafemural (1×10^5 cells). Then after inoculation, mice received a daily treatment of 40 mg/kg ATRA (i.g.) for 1 to 2 consecutive weeks (intravenous injection) or 4 consecutive weeks (intrafemural injection), and 100 μL PBS liposomes or Clodronate liposomes (i.p.) three time per week. All mice underwent complete necropsy for confirmation of pulmonary metastases.

Ethics statement. Investigation has been conducted in accordance with the ethical standards and according to the Declaration of Helsinki and according to national and international guidelines and has been approved by the authors' institutional review board.

MMPs ELISA

MMP12, MMP13, and MMP9 antigen capture ELISA kits (EIAab, Wuhan Eiaab Science Co., Ltd) were used to assess MMP secretion in RAW264.7 cells supernatants by the manufacturer's instructions.

Statistical analysis

For all parameters measured, the values for all samples in different experimental conditions were averaged, and the SD was calculated. Statistical significance of differences between groups was determined with ANOVA or Student unpaired two-tailed *t* test.

Results

M2 TAMs promote metastasis of osteosarcoma cells *in vivo*

To study the role of macrophages in osteosarcoma metastasis, we injected K7M2 WT osteosarcoma cells together with RAW264.7 macrophage cells into the tail vein of mice and examined the numbers of pulmonary metastatic nodules. Mice transplanted with K7M2 WT and RAW264.7 cells had more metastatic nodules on lung surfaces compared with the control mice transplanted with K7M2 WT cells only (Fig. 1A). No overall weight difference was observed (Fig. 1B), but spleen and liver weights were increased in the RAW264.7 and K7M2 WT combination group when compared with those in the control group. We conclude that RAW264.7 activated immunologic function (Supplementary Fig. S1A and S1B). Histologic examination of micrometastatic lung lesions (Fig. 1C and D) suggests that RAW264.7 macrophage cells enhanced both number and size of metastases of K7M2 WT cells. Furthermore, we found that M2-like TAMs ($F4/80^+CD209^+$) were recruited to metastatic nodes in both groups; moreover, more M2 TAMs were detected in the lungs of the mice injected with both RAW264.7 and K7M2 WT cells than the mice injected with K7M2 WT cells alone. However, M1-like TAMs ($F4/80^+CD86^+$) were undetectable in both groups (Fig. 1E and F). Thus, M2-like TAMs were preferentially recruited to metastatic nodes. Neither cell type was detectable in the spleen in either group (Supplementary Fig. S1C). Thus, M2-skewed TAM polarization is attributable to enhanced metastasis of osteosarcoma cells.

ATRA inhibits M2 polarization of macrophages *in vitro*

Because accumulation of M2 TAMs correlates with tumor metastasis, we asked whether ATRA affected polarization of macrophages. We treated RAW264.7 cells with IL13 or IL4 alone or together with 1 μmol/L ATRA, and then determined the expression of $CD206^+$ (M2 marker) by flow cytometers. ATRA did not affect proliferation or viability of macrophages (Supplementary Fig. S2A and S2B). Stimulation either with IL13 or IL4 induced M2-type macrophages (25). The percentage of $CD206^+$ cells increased from 1.56% ± 0.75% in control cells to 49.5% ± 1.96% in IL13-treated cells and 51.0% ± 0.67% in IL4-treated cells (Fig. 2A). ATRA decreased IL13 or IL4 induced CD206 expression, from 49.5% ± 1.96% in the IL13 group to 7.46% ± 0.08% in the IL13 and ATRA combination group, and from 51.0% ± 0.67% in the IL4 group to 9.44% ± 0.52% in the IL4 and ATRA combination group. *MRC-1* and *PPAR-γ* mRNA levels were reduced when ATRA was added (Fig. 2B). Similar results were also obtained in primary bone marrow–derived macrophages (BMDM). Upregulated expression of genes encoding of CD206 and M2 markers (*MRC-1* and *PPAR-γ*) induced by IL13 or IL4 was blocked by ATRA treatment (Fig. 2C). Thus, ATRA inhibited M2-like polarization of macrophages *in vitro*.

We asked whether ATRA could affect M2 polarization of macrophages induced by osteosarcoma tumor cell CM. After K7M2 WT CM treatment, 39.4% ± 13.4% of RAW264.7 cells were $CD206^+$ (Fig. 2E). However, ATRA treatment reduced that percentage to 13.9% ± 2.35%. ATRA had a reverse effect on prestimulated for M2 TAM 48 hours with IL13 or IL4. Our results showed that ATRA could also reverse prepolarization M2 TAMs (Fig. 2F).

We investigated the effect of ATRA in M1 polarization of macrophages. In RAW264.7 cells, ATRA further increased the percentage of $CD86^+$ cells and the mRNA expression of M1 marker genes (*CCL3* and *CCL5*) induced by IFNγ or LPS (Supplementary Fig. S2C and S2D). In BMDM cells, ATRA had no effect on IFNγ or LPS induced M1-like polarization of macrophages (Supplementary Fig. S2E and S2F). Thus, we conclude that ATRA skewed TAM polarization away from the M2-like phenotype *in vitro*.

ATRA eliminates migration-promoting feature of M2 macrophages

We investigated the impact of ATRA on the migration-promoting feature of M2 macrophages. We found no effect of various CMs on survival or proliferation of K7M2 WT cells treated with RM for 24 hours (Supplementary Fig. S3A). We did, however, find that both RM and BM from IL13- or IL4-treated macrophages promoted the invasion of K7M2 WT cells. We used a Matrigel

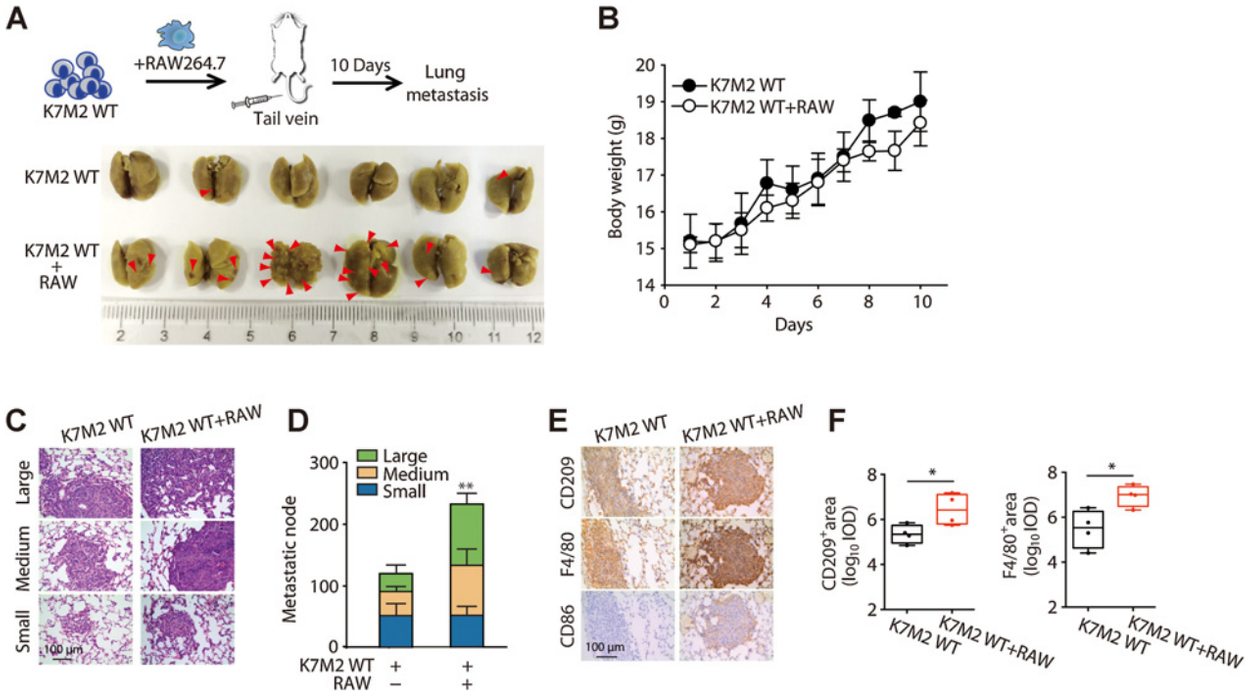

Figure 1.

M2 macrophages promote the metastasis of osteosarcoma. K7M2 WT cells alone or mixed with RAW264.7 cells were tail vein injected into mice and the metastatic nodules were detected. **A,** Experimental outline (top). Photographs of lungs in each mouse (lower). Red arrows indicate metastatic nodules. **B,** The changes of body weight of the mice. **C** and **D,** Quantitative analysis of lung metastatic nodules. **C,** H&E staining of lungs from each mouse. Representative images are shown. **D,** The number of metastatic nodules was counted. Lung metastatic nodules were assigned to three groups according to the diameter: Large, > 400 μm; medium, 200–400 μm; small, < 200 μm. **, $P < 0.01$ by unpaired two-tailed *t* test. **E** and **F,** Immunohistochemical staining of F4/80, CD209, and CD86 in the metastatic tumor tissues. **E,** Representative images. **F,** Quantification of $CD209^+$ and $F4/80^+$ areas in lungs. *, $P < 0.05$ by an unpaired two-tailed *t* test. Results are expressed as mean ± SD of one of at least two independent experiments done ($n = 6$ mice).

invasion assay, in which pores of Transwell plates block migration of noninvasive cells whereas invasive cells degrade the matrix and move through the Matrigel layer. RM and BM collected from cells treated with ATRA in addition to IL13 or IL4 and ATRA did not promote migration of K7M2 WT cells (Fig. 3A–D).

We also evaluated the effect of CM on migration of K7M2 WT cells. Cells seeded in medium in the upper part can migrate downward through pores of the membrane into the lower compartment, in which CM is present. We found that ATRA blocked this migration (Supplementary Fig. S3B–S3E). ATRA also delayed wound closure compared with IL13 or IL4 mono treatment (Fig. 3E–H). Taken together, these results indicate that ATRA might inhibit migration of M2-like macrophages.

We also determined the effect of CM on cell migration and wound-closure ability of human osteosarcoma cell lines (KHOS/NP and U2OS). IL13-induced RAW264.7 cells promoted cell migration and wound-closure ability of human osteosarcoma cells, but ATRA abrogated IL13's effect (Supplementary Fig. S4B–S4D) without any cytotoxicity (Supplementary Fig. S4A). Thus, although M2-like macrophages regulated metastasis for both mouse and human osteosarcoma cells, the effect could be antagonized by ATRA.

ATRA inhibited metastasis of osteosarcoma cells *in vivo*

To evaluate the effect of ATRA in metastasis of osteosarcoma *in vivo*, we used an intravenous injection mouse model. In order to verify whether TAMs played a role in the metastasis process of osteosarcoma cells, we also used clodronate liposomes to chemically eliminate TAMs (26). At first, treatment with either ATRA, clodronate liposomes, or combination did not affect the body weights of the mice (Fig. 4A). We counted the number of macroscopic metastases on the lung surfaces of the mice transplanted with K7M2 WT cells, and the results showed that the number of macroscopic metastases in the mice treated with ATRA was 60% reduced in week 1 and 95% reduced in week 2 when compared with control mice (Fig. 4B and C). Histologic examination was further used to count the number of micrometastatic lesions in lung tissues of the mice transplanted for 1 week, and similar results were also observed (Fig. 4D). Lung metastasis of osteosarcoma cells was reduced in the clodronate liposomes treated mice, and clodronate liposomes could not synergize with ATRA to inhibit metastasis of osteosarcoma cells (Fig. 4A–C). Considering clodronate liposomes achieved 80% to 90% macrophages ($F4/80^+$ cells) depletion in spleen (Fig. 4E and F), our results indicated that ATRA could not further affect metastasis after the elimination of TAMs. Moreover, $F4/80^+CD209^+$ (M2-like) TAMs were recruited to the lung metastasis in the control group, whereas ATRA and clodronate liposomes caused 37.0% and 43.0% reductions in M2 TAMs, respectively (Fig. 4G and H). These data suggest that ATRA could suppress pulmonary metastases of osteosarcoma via inhibiting M2 polarization of TAMs.

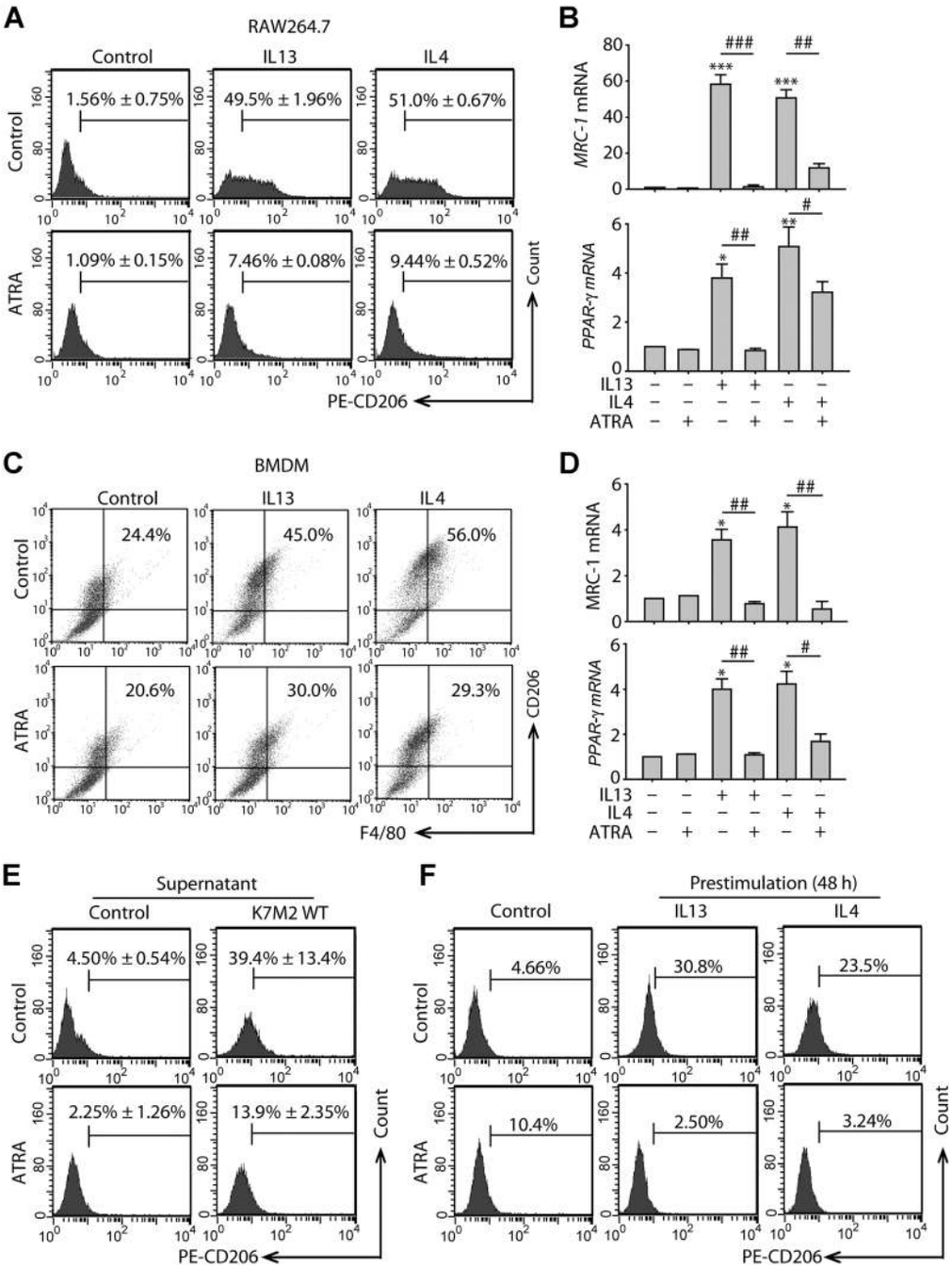

Figure 2.

ATRA inhibited M2 polarization of macrophages. **A,** Flow cytometric analysis of CD206$^+$ cells in RAW264.7 cells treated with IL13 and IL4 in the absence or presence of 1 μmol/L ATRA. Data represent mean ± SD from three independent experiments. **B,** The mRNA levels of *MRC1* and *PPAR-γ* in RAW264.7 cells treated with IL13 and IL4 alone or with 1 μmol/L ATRA. Data represent mean ± SD from three independent experiments. ***, $P < 0.001$ by an unpaired two-tailed *t* test (vs. untreated). #, $P < 0.05$; ##, $P < 0.01$; ###, $P < 0.001$ by an unpaired two-tailed *t* test (vs. combination). **C,** Flow cytometric analysis of F4/80$^+$CD206$^+$ cells in BMDM cells treated with IL13 and IL4 in the absence or presence of 1 μmol/L ATRA. These data were generated from a single experiment. **D,** The mRNA levels of *MRC1* and *PPAR-γ* in BMDM cells treated with IL13 and IL4 in the absence or presence of 1 μmol/L ATRA. Data represent mean ± SD from three independent experiments. *, $P < 0.05$ by an unpaired two-tailed *t* test (vs. untreated). #, $P < 0.05$; ##, $P < 0.01$ by an unpaired two-tailed *t* test (vs. combination). **E,** Flow cytometric analysis of CD206$^+$ cells in RAW264.7 cells treated with the supernatant of K7M2 WT cells in the absence or presence of 1 μmol/L ATRA for 48 hours. Data represent mean ± SD from three independent experiments. **F,** Flow cytometric analysis of CD206$^+$ cells in RAW264.7 cells pretreated with IL13 and IL4 for 48 hours followed by ATRA treatment for another 48 hours. These data were generated from a single experiment.

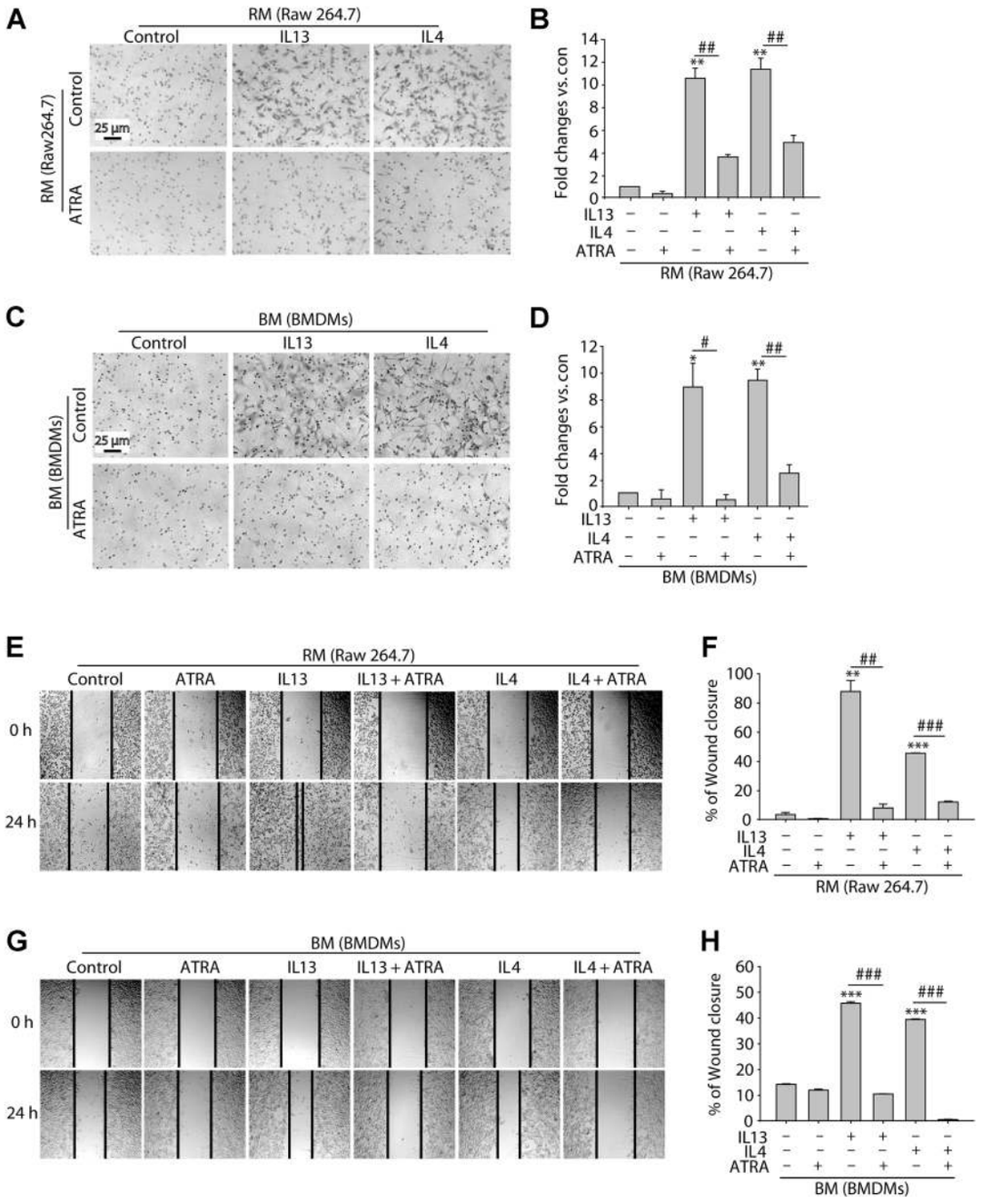

Figure 3.

ATRA abrogates migration-promoting feature of M2 macrophages. **A–D,** ATRA inhibited RM (**A–B**) or BM (**C–D**) enhanced invasion of K7M2 WT cells. K7M2 WT cells were treated with RM or BM for 24 hours, and the cell invasion ability was determined by Matrigel invasion assay. **A** and **C,** Representative images are shown. **B** and **D,** Quantitative analysis of invaded K7M2 WT cells. Results are expressed as mean ± SD from three independent experiments of two biological replicates. *, $P < 0.05$; **, $P < 0.01$ by an unpaired two-tailed *t* test (vs. untreated control). #, $P < 0.05$; ##, $P < 0.01$ by an unpaired two-tailed *t* test (vs. combination). **E–H,** ATRA caused a delay in wound closure of K7M2 WT cells. K7M2 WT cells were treated with RM (**E–F**) or BM (**G–H**) for 24 hours with straight scratches, and the migration of cells across this artificial wound was assessed. **E** and **G,** Representative images are shown. **F** and **H,** Quantitative analysis of the wound area. Gap size at 0 hour was set to 100% and percentage of closed wound was calculated after 24 hours after image analysis. Bars, mean ± SD ($n = 3$). **, $P < 0.01$; ***, $P < 0.001$ by an unpaired two-tailed *t* test (vs. untreated control). ##, $P < 0.01$; ###, $P < 0.001$ by an unpaired two-tailed *t* test (vs. combination).

We evaluated the antimetastasis effect of ATRA in an orthotopic transplantation mouse model (Fig. 5A). ATRA treatment reduced lung metastases by 85.8% ($P < 0.01$ vs. control), and clodronate liposomes reduced metastases by 67.6% ($P < 0.05$ vs. control; Fig. 5B). After ATRA treatment, no large pulmonary metastatic nodes (diameter > 400 μm) were observed in the lungs, and only a

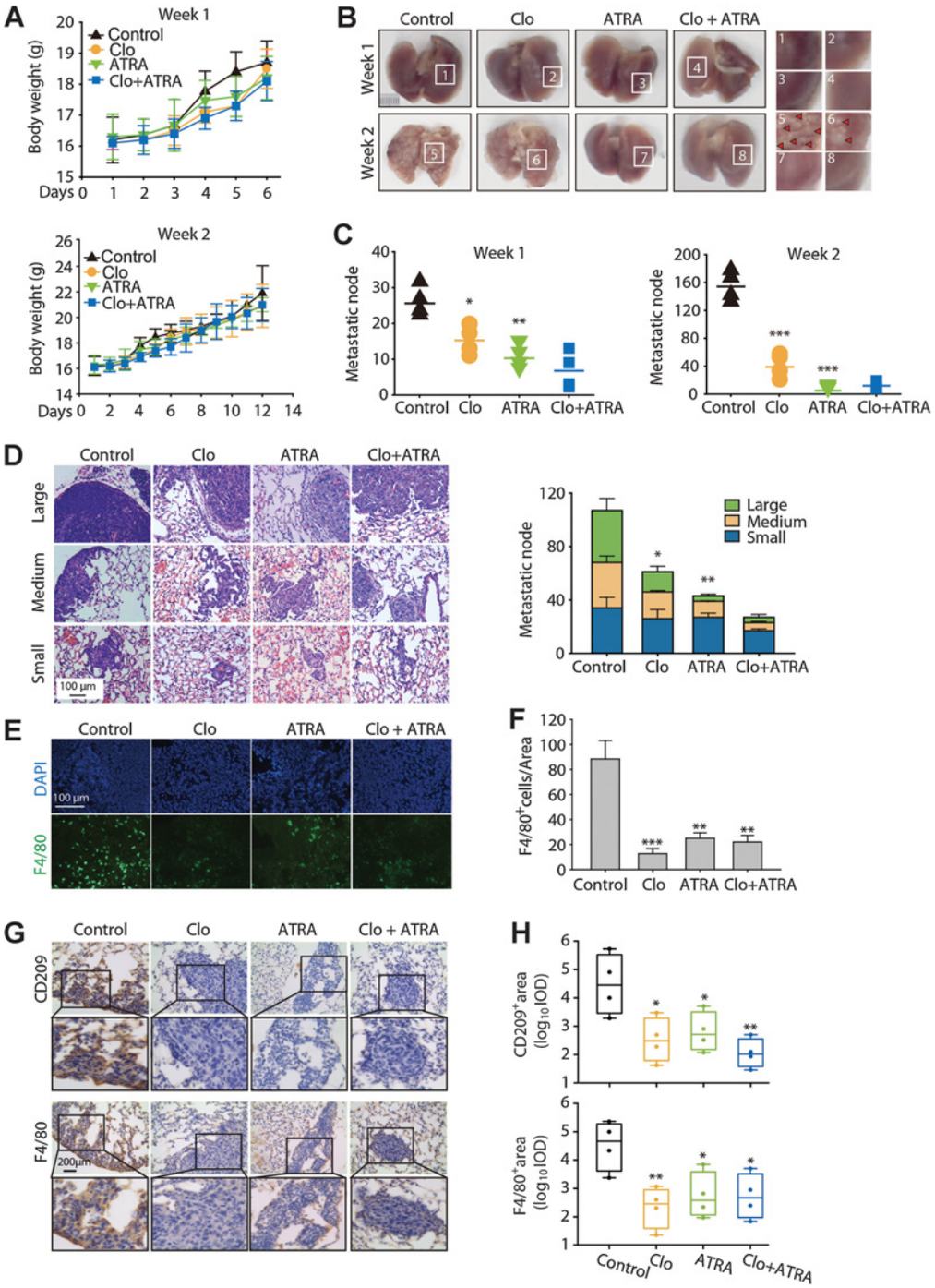

Figure 4.

ATRA decreased lung metastasis of osteosarcoma in an intravenous injection mouse model. Balb/c mice were intravenously injected with 1×10^6 K7M2 WT cells. One or two weeks after infection, mice were euthanized to determine the metastatic nodules on the lungs. **A,** The changes of body weight of the mice. **B,** Representative images of the lungs. **C,** Quantitative analysis of lung metastasis nodules on the surfaces of the lungs of the mice. *, $P < 0.05$; **, $P < 0.01$; ***, $P < 0.001$ by an unpaired two-tailed *t* test (vs. control). **D,** H&E staining of lung metastatic nodules (week 1 group). Representative images are shown (left). The numbers of metastatic nodules were counted. *, $P < 0.05$; **, $P < 0.01$ an unpaired two-tailed *t* test (vs. control). **E** and **F,** Immunofluorescence analysis of F4/80$^+$ TAMs in the spleen of mice (week 1 group). **E,** Representative images are shown. **F,** Quantification of the F4/80$^+$ cells in the spleen. **, $P < 0.01$; ***, $P < 0.001$ by an unpaired two-tailed *t* test (vs. control). **G** and **H,** Immunohistochemical staining of F4/80 and CD209 in the metastatic tumor tissues of mice (week 1 group). **G,** Representative images are shown. **H,** Quantification of the CD209$^+$ and F4/80$^+$ areas in lungs. *, $P < 0.05$; **, $P < 0.01$ by an unpaired two-tailed *t* test (vs. control). These data were generated from two independent experiments with two time points ($n = 4$ mice).

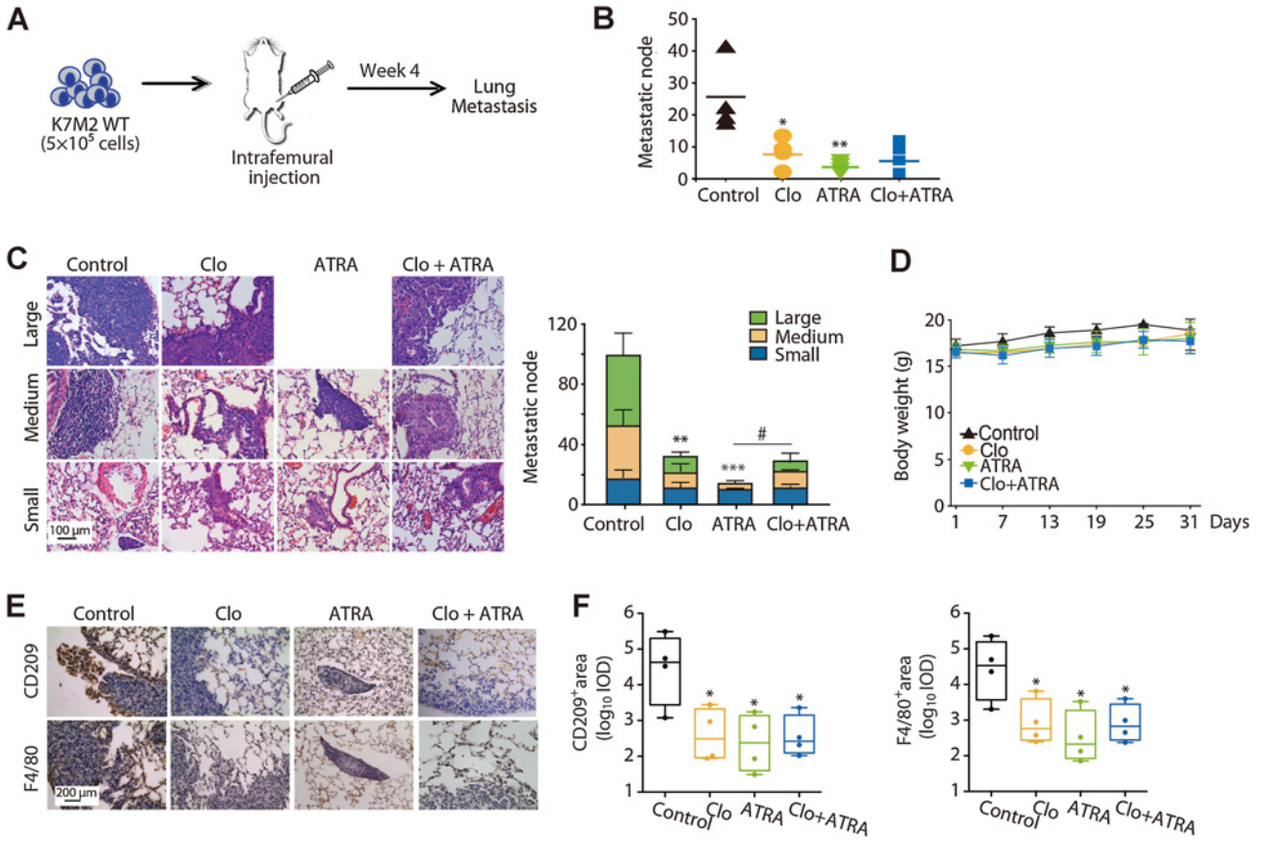

Figure 5.

ATRA inhibited the metastasis of osteosarcoma in an orthotropic mouse model. Balb/c mice were intrafemurally injected with 5×10^5 K7M2 WT cells and euthanized to determine the metastatic nodules on the lungs. $n = 4$ mice. **A,** Experimental outline. **B,** Quantitative analysis of lung metastatic nodules on the surfaces of the lungs of the mice. *, $P < 0.05$; **, $P < 0.01$ by an unpaired two-tailed t test (vs. control). **C,** H&E staining of lung metastatic nodules. Representative images are shown (left). The numbers of metastatic nodules were counted. *, $P < 0.05$; **, $P < 0.01$ by an unpaired two-tailed t test (vs. control). #, $P < 0.05$ by an unpaired two-tailed t test (vs. combination). **D,** The changes of body weight of the mice. **E** and **F,** Immunohistochemical staining of F4/80 and CD209 in the metastatic tumor tissues. **E,** Representative images are shown. **F,** Quantification of the $CD209^+$ and $F4/80^+$ area in lungs. *, $P < 0.05$ by an unpaired two-tailed t test (vs. control). These data were generated from a single experiment ($n = 4$).

few medium metastatic nodes were found. However, many metastatic nodes of various sizes appeared in control mice (Fig. 5B and C). ATRA did not affect the body weight of the mice (Fig. 5D), but inhibited the polarization of M2-type TAMs (Fig. 5E and F). We conclude that ATRA inhibited pulmonary metastasis of osteosarcoma cells through a mechanism that skews macrophages toward the M2 phenotype.

ATRA blocks activation of gene transcription related to M2 polarization

To understand the mechanisms involved, we asked whether ATRA could affect several transcription factors or signaling pathways required for macrophages to switch their polarization to M2, such as STAT3/6 phosphorylation (27, 28), C/EBPβ activation (17, 29), and JNK signal pathway (24). ATRA did not inhibit activation of STAT3/6, C/EBPβ, and JNK1/2 induced by IL13 and IL4 (Supplementary Fig. S5). We found changes in gene expression by analysis of RNA extracted from RAW264.7 cells treated with IL13 in the absence or presence with ATRA for 12 and 24 hours (Fig. 6A). A total of 1,273 genes (533 upregulated vs. 740 downregulated) showed the same changes in IL13-induced M2-type macrophage cells, and 1,953 genes (655 upregulated vs. 1,298 downregulated) showed the same changes in ATRA-blocked cells. Of the 1,273 altered genes in the IL13-treated group, 192, named as cluster 1, were upregulated in the IL13 group, but had no change or were downregulated in the combination group; 132 genes, named as cluster 2, were downregulated in the IL13 group, but had no change or were upregulated in the combination group (Supplementary Table S1).

These 324 inversely altered genes were visualized with TreeView (Fig. 6B) and submitted to David functional annotation clustering analysis (Supplementary Table S2). The results revealed that these changed genes were involved in secreted factors (89), vasculature development (26), apoptosis (36), inflammatory response (16), cell adhesion (27), cell junction (31), cell migration (16), cell motion (22), and collagen degradation (4). We then selected several M2 macrophage marker genes to explore the effect of ATRA on the transcription program. We found that IL13 activated the transcription of *MRC-1*, *CCL-1*, *IL10*, *IL13RA2*, *MMP13*, *VEGFC*, *CCR2*, and *PPAR-γ*, but ATRA inhibited the transcription of these

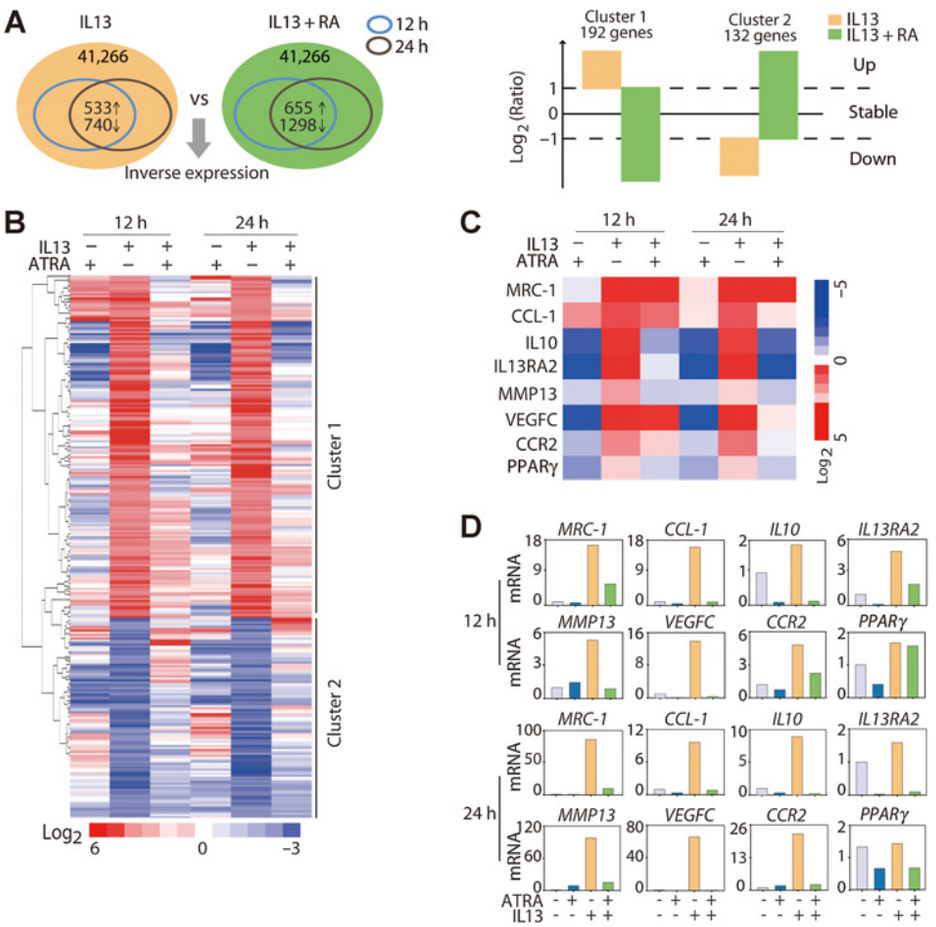

Figure 6.
ATRA blocked the activation of M2 polarization–related gene transcription. **A,** Schematic representation of comparing gene expression profiles in RAW264.7 macrophages. Left, the overlapped smaller circles reflect the shared 1273 genes in the IL13 group (up: 533, down: 740) and 1,953 genes in the IL13 + ATRA group (up: 655, down: 1298), respectively. Right, the inverse expression genes were selected at a cut of Log_2 (Ratio) $\geq$ 2.0 or $\leq$ 0.5. **B,** Heatmap display of hierarchical clustering of 324 overlapped genes sorted from **A**. **C,** Heatmap display of M2-related genes. **D,** Real-time PCR validation of M2-related genes in RAW264.7 cells treated with IL13 alone or with ATRA. Results are expressed as mean of a single experiment done in triplicates.

genes (Fig. 6C). Real-time PCR was used to verify the inhibition effect of ATRA on the M2 polarization of macrophages (Fig. 6D). Therefore, our results suggest that ATRA could block activation of M2 polarization–related transcription induced by IL13.

ATRA blocks secretion of MMP12 in M2 TAMs to slow metastasis

M2 TAMs regulate tumor cell migration/invasion through secreting proangiogenic factors (30, 31). We focused on the changes of proangiogenic factors to understand the mechanism of the antimetastasis effect of ATRA. We found that ATRA could antagonize IL13-induced upregulation of secreted factors and metastasis-related factors which were involved in vasculature development, cell migration, cell junction, and collagen degradation (Fig. 7A). Migration on and through extracellular matrix is a necessary aspect of cell migration. Matrix metalloproteinases (MMP) are a family of zinc-dependent enzymes that can degrade the extracellular matrix (32). ATRA regulates MMP9 production in macrophages (33). Because we found MMP12, MMP13, and MMP14 variable in IL13 and IL13 plus ATRA groups (Fig. 7A), we focused on regulation of MMPs. Real-time PCR was further performed to verify the changes of those three genes. *MMP12* and *MMP13* showed inverse expression patterns between IL13 and IL13 plus ATRA groups upon 12- and 24-hour treatment, whereas *MMP14* and *MMP9* did not (Fig. 7B). ELISA results demonstrated that IL13 enhanced secretion of MMP12 in RAW264.7 cells (12 hours: 332.6 pg/mL in IL13 vs. 65.0 pg/mL in control; 24 hours: 658.7 pg/mL in IL13 vs. 175.7 pg/mL in control). The secretion was blocked by ATRA (216.7 pg/mL in 12 hours, and 319.8 pg/mL in 24 hours; Fig. 7C), which was consistent with our microarray and RT-PCR results. ATRA did not block secretion of MMP13 induced by IL13 at 12 and 24 hours, and only blocked 25% MMP13 secretion at 48 hours (Fig. 7C). The production of MMP9 was also not enhanced by IL13. Instead, ATRA had a stimulation effect on the production of MMP9 (Fig. 7C), suggesting that MMP9 is not responsible for ATRA's antimetastasis effect. Thus, ATRA inhibited secretion of MMP12 induced by IL13 in RAW264.7 cells.

We evaluated the effect of MMPs on the invasion of K7M2 WT cells by using mmp408, a biosynthesis inhibitor which is profiled for cross-species MMP12 activity (34). mmp408 inhibits human MMP12, but is 50 times less effective against mouse MMP12. Therefore, we used mmp408 at 160 nmol/L, a concentration reported to inhibit mouse MMP12, to treat K7M2 WT cells. We confirmed that mmp408 did not affect proliferation and survival of K7M2 WT cells (Supplementary Fig. S6A). mmp408 abrogated the invasion-promoting effect of IL13 or IL4 induced M2-like macrophages in K7M2 WT cells (Fig. 7D and E), indicating that inhibition of secretion of MMP12 or other MMPs may be critical to the antimetastatic effect of ATRA. We then introduced antibodies to MMP9 and MMP12 to functionally neutralize the activity of MMP9 and MMP12. The MMP12 antibody abrogated RM-enhanced invasion ability of K7M2 WT cells, whereas the

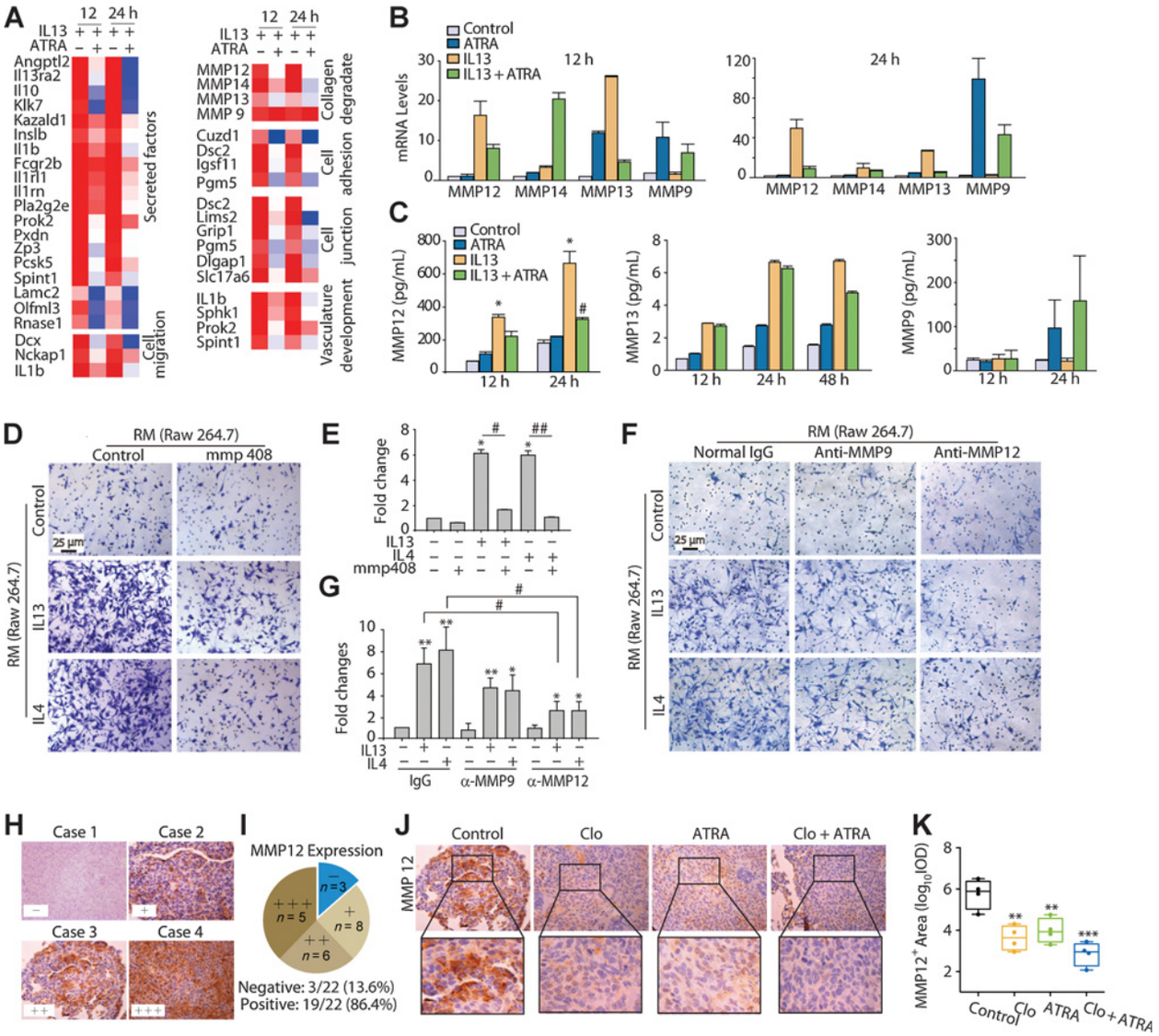

Figure 7.

Inhibiting the secretion of MMP12 in M2 macrophages is critical to ATRA's antimetastatic effect. **A,** Heatmap display of annotation cluster of secreted factors and metastasis-related factors. **B,** Real-time PCR validation of the *MMP12, MMP13, MMP14,* and *MMP9* genes in RAW264.7 cells treated with IL13 alone or with 1 μmol/L ATRA for 12 and 24 hours, respectively. Data, mean ± SD from three independent experiments. **C,** Determination of MMP12, MMP13, and MMP9 secretion by ELISA in conditioned supernatants of RAW264.7 cells. Data, mean ± SD from three independent experiments. *, $P < 0.05$ by an unpaired two-tailed *t* test (vs. untreated control). #, $P < 0.05$ by an unpaired two-tailed *t* test (vs. IL13 treatment). **D** and **E,** mmp408 inhibited the invasion of K7M2 WT cells. K7M2 WT cells were treated with RM in the presence of 160 nmol/L mmp408 for 24 hours, and the cell invasion ability was determined by Matrigel invasion assay. **D,** Representative images are shown. **E,** Quantitative analysis of invaded K7M2 WT cells. Bars, mean ± SD ($n = 3$). *, $P < 0.05$ by an unpaired two-tailed *t* test (vs. untreated control). #, $P < 0.05$; ##, $P < 0.01$ by an unpaired two-tailed *t* test (vs. combination). **F** and **G,** The effect of anti-MMP9 and anti-MMP12 antibodies on the invasion of K7M2 WT cells. K7M2 WT cells were treated with RM in the presence of anti-MMP9 or anti-MMP12 antibodies for 24 hours and the cell invasion ability was determined by Matrigel invasion assay. **F,** Representative images are shown. **G,** Quantitative analysis of invaded K7M2 WT cells. Bars represent mean ± SD ($n = 3$). *, $P < 0.05$; **, $P < 0.01$ by an unpaired two-tailed *t* test (vs. untreated control). #, $P < 0.05$ by an unpaired two-tailed *t* test (vs. combination). **H** and **I,** Immunohistochemical staining of MMP12 in metastatic tumor tissues. **H,** Four representative cases with different MMP12 expression levels were shown. **I,** The expression levels of MMP12 in 22 detected osteosarcoma tumor tissues were graded and summarized in pie charts. "−": negative; "+": low; "++": medium; "+++": high positive. **J** and **K,** Immunohistochemical staining of MMP12 in metastatic lung tissues of the mice treated with clodronate liposomes or/and ATRA. **J,** Representative images are shown. **K,** Quantification of the $MMP12^+$ area in lungs. **, $P < 0.01$; ***, $P < 0.001$ by an unpaired two-tailed *t* test (vs. control).

MMP9 antibody did not (Fig. 7F and G). Thus, ATRA may affect production of MMP12 by M2 macrophages, reducing their ability to invade osteosarcoma cells.

We determined the MMP12 expression in murine osteosarcoma metastatic tissues by immunohistochemistry assay. Four representative cases with different MMP12 expression levels were

shown (Fig. 7H). As indicated in Fig. 7I, 19 of 22 osteosarcoma cases (86.4%) showed MMP12 immunoreactivities, indicating the importance of MMP12 in osteosarcoma. We found that ATRA reduced expression of MMP12 in metastatic tumor tissues of the mice treated with clodronate liposomes and ATRA when compared with the control (Fig. 7J and K). Altogether, our results suggest that inhibiting the secretion of MMP12 in M2 macrophages is critical to ATRA's antimetastatic effect in osteosarcoma cells.

Discussion

M2 TAMs play a critical role in cancer metastasis (35, 36) and could potentiate metastatic cells. Here, we demonstrated that M2 polarization of TAMs promoted pulmonary metastasis of osteosarcoma cells. This result suggested that M2 macrophages might be appropriate targets for antimetastasis therapy of osteosarcoma patients. We established that ATRA inhibited M2 polarization of macrophages and could abrogate pulmonary metastasis of osteosarcoma through reducing the infiltration of M2-type macrophages *in vivo*. Our results identified ATRA as a promising agent to target M2 macrophages for future antimetastasis therapy of osteosarcoma.

M2 TAMs represent an attractive target of biological therapies for cancers. Trabectedin (ET-743), a licensed anticancer agent, is selectively cytotoxic for TAMs, thus engaging macrophage intervention in therapeutic settings (37). Preventing cancer metastasis through inhibiting M2-type macrophages might be an attractive and feasible strategy in cancer therapeutics. ATRA inhibits tumor invasion and metastases (22, 38). Myeloid-derived suppressor cells (MDSC) promote tumor angiogenesis and metastasis (39); ATRA could induce differentiation of MDSCs (40). Administration of ATRA to patients with metastatic renal-cell carcinoma resulted in a substantial decrease in the number of MDSCs and improved antigen-specific response of T cells and metastatic disease (41). Hence, MDSCs are potential targets for ATRA in cancer therapeutics. Here, we reported that ATRA could reduce pulmonary metastatic nodes of osteosarcoma and attributed this effect to inhibition of M2-type macrophages. As MDSCs share some properties and gene expression profiles with M2 TAMs, it is likely that, by nature, MDSCs skew toward the M2 orientation. However, the MDSCs are complex. Study of the connection between MDSCs and M2 TAMs is warranted. Our *in vivo* study found that ATRA decreases the number of macrophages, as the number of $F4/80^+$ cells decrease in both spleen and lungs after ATRA treatment, which suggests that ATRA may deplete macrophages *in vivo*. However, both our *in vitro* and other's studies suggest that ATRA was not toxic to macrophages (23). Considering that ATRA can induce tissue-specific localization and functional polarization of macrophages (42), we cannot rule out the possibility that ATRA may affect the recruitment or localization of macrophages *in vivo*.

TAMs in tumors may be derived from circulating monocytes or resident macrophages. TAMs are almost entirely derived from peripheral blood monocytes recruited into the tumor from the local circulation (rather than resident macrophages; refs. 43, 44). Glioma stem cells recruit TAMs and support the tumor-promoting M2 subtypes, indicating a preferential recruitment of peripheral macrophages (45). Despite indications that resident macrophages are not critical, both resident microglia and blood-derived monocytes generate the pool of macrophages that infiltrate brain tumors of either primary or metastatic origin (46). Therefore, both resident and recruited macrophages regulate neoplastic cell proliferation, survival, and invasion. Future work should focus on exploring the full spectrum of macrophage polarization, uncovering mechanisms of transformation of polarization, and finding the approach to target macrophages for tumor therapeutics. Our study found that ATRA prevents migration of osteosarcoma cells via blocking the M2 polarization of TAMs. Thus, we propose that ATRA is a promising antimetastatic agent for osteosarcoma therapeutics.

We used both a long-term established RAW264.7 cell line and primary macrophages (BMDMs) for *in vitro* experiments. The RAW264.7 cell line was established from murine tumors induced by Abelson leukemia virus; these tumors express properties of macrophages (47). How this might affect ATRA's response remains unclear. Further studies using other macrophage cell lines or a better cell model, such as macrophages isolated from tumor-bearing lungs, are needed to confirm our hypothesis.

Studies have shed new light on the transcriptional mechanisms of macrophage development and activation (27). The STAT3/6 family and the nuclear receptor PPAR-γ are transcription factors that translate signals and polarize macrophages into M2 phenotype. We found that STAT3/6 and C/EBPβ were not regulated by ATRA (Supplementary Fig. S5). However, PPAR-γ was activated by IL13, whereas ATRA inhibited the activation. Therefore, PPAR-γ is a regulator of M2 polarization of macrophages. Further studies on the specific role of PPAR-γ in ATRA-inhibited M2 TAM are required.

Tumor metastasis and invasion of secondary organs or tissues requires that physical barriers, such as the endothelial basement membrane, be crossed. MMPs are endopeptidases with the ability to degrade extracellular matrix protein and facilitate tumor cell metastasis (48). In our microarray study, mRNA levels of *MMP9*, *MMP12*, *MMP13*, and *MMP14* were regulated by IL13. However, RT-PCR and ELISA results confirmed downregulation by ATRA during the M2 polarization process only for MMP12. MMP12 is an elastolytic metalloproteinase secreted by inflammatory macrophages (49). In many cancers, MMP12 expression correlates with metastatic phenotype, such as non–small cell lung cancer (50), hepatocellular carcinoma (51), and squamous cell cancer (52). MMP12 is also amplified in osteosarcoma (53). Our immunohistochemistry staining results showed expression of MMP12 in tumor metastatic nodes (control group). ATRA treatment decreased the expression of MMP12. The antibody against MMP12 could abrogate RM-enhanced invasion ability of K7M2 WT cells. These results suggested that MMP12 might affect ATRA-controlled M2 polarization and ATRA-inhibited osteosarcoma metastasis. However, ATRA also encourages production of MMP9 in macrophages (23, 33). Our results agree with the finding that ATRA alone can stimulate the production of MMP9 (33). The effect of IL13 is very weak, suggesting that MMP9 may not responsible for the antimetastatic effect of ATRA on M2 TAMs. We used the antibody against MMP9 in the invasion assay, and the results indicated that anti-MMP9 antibody had an inhibitory effect on the invasion of K7M2 WT cells induced by CM (32.0% and 45.7% inhibition in the IL13 and IL4 groups, respectively), but the effect of anti-MMP12 antibody is much stronger (62.4% and 68.6% inhibition in the IL13 and IL4 groups, respectively). RAW264.7 cells release more MMP12 than MMP9, whereas K7M2 WT cells secrete more MMP9 than MMP12 (Supplementary Fig. S6B and S6C), which could explain this

phenomenon. Thus, we hypothesize that MMP 9 is more important in K7M2 WT cells, and MMP12 is responsible for the effect of macrophages.

In summary, we demonstrate that M2 polarization of macrophages promotes pulmonary metastasis of osteosarcoma cells, whereas ATRA discourages metastasis by inhibiting M2-like macrophages. Our results link TAM to the antimetastatic effect of ATRA. Our findings may lead to clinical applications of ATRA to target TAMs for osteosarcoma metastasis intervention.

Disclosure of Potential Conflicts of Interest

No potential conflicts of interest were disclosed.

Authors' Contributions

Conception and design: Q. Zhou, M. Ying, Q. He
Development of methodology: Q. Zhou, M. Xian, X. Yang, M. Ying
Acquisition of data (provided animals, acquired and managed patients, provided facilities, etc.): Q. Zhou, M. Xian, S. Xiang, D. Xiang, X. Shao, J. Wang
Analysis and interpretation of data (e.g., statistical analysis, biostatistics, computational analysis): J. Cao, B. Yang, M. Ying, Q. He
Writing, review, and/or revision of the manuscript: J. Cao, B. Yang, M. Ying, Q. He
Administrative, technical, or material support (i.e., reporting or organizing data, constructing databases): B. Yang, M. Ying, Q. He
Study supervision: M. Ying, Q. He

Acknowledgments

We would like to acknowledge Renhua Gai, Jian Ma, and Honghai Wu from the Center for Drug Safety Evaluation and Research of Zhejiang University for outstanding technical assistance.

Grant Support

This work was supported by grants from the National Natural Science Foundation of China (No. 81573453 to X.C. Yang, No. 81625024 and No. 91529304 to B. Yang, No. 81473225 to Q.J. He), International Science & Technology Cooperation Program of China (No. 2014DFE30050 to B. Yang), the Fundamental Research Funds for the Central Universities, and Zhejiang Provincial Program for the cultivation of High-level Innovative Health Talents.

The costs of publication of this article were defrayed in part by the payment of page charges. This article must therefore be hereby marked *advertisement* in accordance with 18 U.S.C. Section 1734 solely to indicate this fact.

Received October 10, 2016; revised February 24, 2017; accepted May 12, 2017; published OnlineFirst May 17, 2017.

References

1. Marina N, Gebhardt M, Teot L, Gorlick R. Biology and therapeutic advances for pediatric osteosarcoma. Oncologist 2004;9:422–41.
2. Bacci G, Ferrari S, Bertoni F, Ruggieri P, Picci P, Longhi A, et al. Long-term outcome for patients with nonmetastatic osteosarcoma of the extremity treated at the istituto ortopedico rizzoli according to the istituto ortopedico rizzoli/osteosarcoma-2 protocol: an updated report. J Clin Oncol 2000; 18:4016–27.
3. Ferguson WS, Goorin AM. Current treatment of osteosarcoma. Cancer Invest 2001;19:292–315.
4. Robinson BD, Sica GL, Liu YF, Rohan TE, Gertler FB, Condeelis JS, et al. Tumor microenvironment of metastasis in human breast carcinoma: a potential prognostic marker linked to hematogenous dissemination. Clin Cancer Res 2009;15:2433–41.
5. Condeelis J, Pollard JW. Macrophages: obligate partners for tumor cell migration, invasion, and metastasis. Cell 2006;124:263–6.
6. Pollard JW. Tumour-educated macrophages promote tumour progression and metastasis. Nat Rev Cancer 2004;4:71–8.
7. Mantovani A, Sozzani S, Locati M, Allavena P, Sica A. Macrophage polarization: tumor-associated macrophages as a paradigm for polarized M2 mononuclear phagocytes. Trends Immunol 2002;23:549–55.
8. Pollard JW. Macrophages define the invasive microenvironment in breast cancer. J Leukoc Biol 2008;84:623–30.
9. Nonomura N, Takayama H, Nakayama M, Nakai Y, Kawashima A, Mukai M, et al. Infiltration of tumour-associated macrophages in prostate biopsy specimens is predictive of disease progression after hormonal therapy for prostate cancer. BJU Int 2011;107:1918–22.
10. Bailey C, Negus R, Morris A, Ziprin P, Goldin R, Allavena P, et al. Chemokine expression is associated with the accumulation of tumour associated macrophages (TAMs) and progression in human colorectal cancer. Clin Exp Metastasis 2007;24:121–30.
11. Osinsky S, Bubnovskaya L, Ganusevich I, Kovelskaya A, Gumenyuk L, Olijnichenko G, et al. Hypoxia, tumour-associated macrophages, microvessel density, VEGF and matrix metalloproteinases in human gastric cancer: interaction and impact on survival. Clin Transl Oncol 2011; 13:133–8.
12. Mantovani A, Sica A. Macrophages, innate immunity and cancer: balance, tolerance, and diversity. Curr Opin Immunol 2010;22:231–7.
13. Franklin RA, Li MO. The ontogeny of tumor-associated macrophages: a new understanding of cancer-elicited inflammation. Oncoimmunology 2014;3:e955346.
14. Buddingh EP, Kuijjer ML, Duim RA, Burger H, Agelopoulos K, Myklebost O, et al. Tumor-infiltrating macrophages are associated with metastasis suppression in high-grade osteosarcoma: a rationale for treatment with macrophage activating agents. Clin Cancer Res 2011; 17:2110–9.
15. Ying M, Zhang L, Zhou Q, Shao X, Cao J, Zhang N, et al. The E3 ubiquitin protein ligase MDM2 dictates all-trans retinoic acid-induced osteoblastic differentiation of osteosarcoma cells by modulating the degradation of RARalpha. Oncogene 2016;35:4358–67.
16. Wansley DL, Yin Y, Prussin C. The retinoic acid receptor-alpha modulators ATRA and Ro415253 reciprocally regulate human IL-5+ Th2 cell proliferation and cytokine expression. Clin Mol Allergy 2013;11:4.
17. Cavnar MJ, Zeng S, Kim TS, Sorenson EC, Ocuin LM, Balachandran VP, et al. KIT oncogene inhibition drives intratumoral macrophage M2 polarization. J Exp Med 2013;210:2873–86.
18. Ji Y, Sun S, Xu A, Bhargava P, Yang L, Lam KS, et al. Activation of natural killer T cells promotes M2 Macrophage polarization in adipose tissue and improves systemic glucose tolerance via interleukin-4 (IL-4)/STAT6 protein signaling axis in obesity. J Biol Chem 2012;287:13561–71.
19. Yuan F, Fu X, Shi H, Chen G, Dong P, Zhang W. Induction of murine macrophage M2 polarization by cigarette smoke extract via the JAK2/STAT3 pathway. PLoS One 2014;9:e107063.
20. Liu H, Zang C, Fenner MH, Possinger K, Elstner E. PPARgamma ligands and ATRA inhibit the invasion of human breast cancer cells in vitro. Breast Cancer Res Treat 2003;79:63–74.
21. Wu Q, Chen YQ, Chen ZM, Chen F, Su WJ. Effects of retinoic acid on metastasis and its related proteins in gastric cancer cells in vivo and in vitro. Acta Pharmacol Sin 2002;23:835–41.
22. Oldridge EE, Walker HF, Stower MJ, Simms MS, Mann VM, Collins AT, et al. Retinoic acid represses invasion and stem cell phenotype by induction of the metastasis suppressors RARRES1 and LXN. Oncogenesis 2013;2:e45.
23. Tsagozis P, Augsten M, Pisa P. All trans-retinoic acid abrogates the pro-tumorigenic phenotype of prostate cancer tumor-associated macrophages. Int Immunopharmacol 2014;23:8–13.
24. Zhang J, Cao J, Ma S, Dong R, Meng W, Ying M, et al. Tumor hypoxia enhances Non-Small Cell Lung Cancer metastasis by selectively promoting macrophage M2 polarization through the activation of ERK signaling. Oncotarget 2014;5:9664–77.
25. Murray PJ, Allen JE, Biswas SK, Fisher EA, Gilroy DW, Goerdt S, et al. Macrophage activation and polarization: nomenclature and experimental guidelines. Immunity 2014;41:14–20.
26. Germano G, Frapolli R, Belgiovine C, Anselmo A, Pesce S, Liguori M, et al. Role of macrophage targeting in the antitumor activity of trabectedin. Cancer Cell 2013;23:249–62.
27. Lawrence T, Natoli G. Transcriptional regulation of macrophage polarization: enabling diversity with identity. Nat Rev Immunol 2011;11:750–61.

28. Sica A, Mantovani A. Macrophage plasticity and polarization: in vivo veritas. J Clin Invest 2012;122:787–95.
29. Ruffell D, Mourkioti F, Gambardella A, Kirstetter P, Lopez RG, Rosenthal N, et al. A CREB-C/EBPbeta cascade induces M2 macrophage-specific gene expression and promotes muscle injury repair. Proc Natl Acad Sci USA 2009;106:17475–80.
30. Sica A, Allavena P, Mantovani A. Cancer related inflammation: the macrophage connection. Cancer Lett 2008;267:204–15.
31. Mantovani A, Schioppa T, Porta C, Allavena P, Sica A. Role of tumor-associated macrophages in tumor progression and invasion. Cancer Metastasis Rev 2006;25:315–22.
32. Deryugina EI, Quigley JP. Matrix metalloproteinases and tumor metastasis. Cancer Metastasis Rev 2006;25:9–34.
33. Lo HM, Wang SW, Chen CL, Wu PH, Wu WB. Effects of all-trans retinoic acid, retinol, and beta-carotene on murine macrophage activity. Food Funct 2014;5:140–8.
34. Li W, Li J, Wu Y, Wu J, Hotchandani R, Cunningham K, et al. A selective matrix metalloprotease 12 inhibitor for potential treatment of chronic obstructive pulmonary disease (COPD): discovery of (S)-2-(8-(methoxycarbonylamino)dibenzo[b,d]furan-3-sulfonamido)-3-methylbutanoic acid (MMP408). J Med Chem 2009;52:1799–802.
35. Paolino M, Choidas A, Wallner S, Pranjic B, Uribesalgo I, Loeser S, et al. The E3 ligase Cbl-b and TAM receptors regulate cancer metastasis via natural killer cells. Nature 2014;507:508–12.
36. Zarif JC, Taichman RS, Pienta KJ. TAM macrophages promote growth and metastasis within the cancer ecosystem. Oncoimmunology 2014;3:e941734.
37. Allavena P, Germano G, Belgiovine C, D'Incalci M, Mantovani A. Trabectedin: a drug from the sea that strikes tumor-associated macrophages. Oncoimmunology 2013;2:e24614.
38. Cheng J, Qi J, Li XT, Zhou K, Xu JH, Zhou Y, et al. ATRA and Genistein synergistically inhibit the metastatic potential of human lung adenocarcinoma cells. Int J Clin Exp Med 2015;8:4220–7.
39. Murdoch C, Muthana M, Coffelt SB, Lewis CE. The role of myeloid cells in the promotion of tumour angiogenesis. Nat Rev Cancer 2008;8:618–31.
40. Gabrilovich DI, Nagaraj S. Myeloid-derived suppressor cells as regulators of the immune system. Nat Rev Immunol 2009;9:162–74.
41. Mirza N, Fishman M, Fricke I, Dunn M, Neuger AM, Frost TJ, et al. All-trans-retinoic acid improves differentiation of myeloid cells and immune response in cancer patients. Cancer Res 2006;66:9299–307.
42. Okabe Y, Medzhitov R. Tissue-specific signals control reversible program of localization and functional polarization of macrophages. Cell 2014;157:832–44.
43. Yamashiro S, Takeya M, Nishi T, Kuratsu J, Yoshimura T, Ushio Y, et al. Tumor-derived monocyte chemoattractant protein-1 induces intratumoral infiltration of monocyte-derived macrophage subpopulation in transplanted rat tumors. Am J Pathol 1994;145:856–67.
44. Murdoch C, Giannoudis A, Lewis CE. Mechanisms regulating the recruitment of macrophages into hypoxic areas of tumors and other ischemic tissues. Blood 2004;104:2224–34.
45. Zhou W, Ke SQ, Huang Z, Flavahan W, Fang X, Paul J, et al. Periostin secreted by glioblastoma stem cells recruits M2 tumour-associated macrophages and promotes malignant growth. Nat Cell Biol 2015;17:170–82.
46. De Palma M. Origins of brain tumor macrophages. Cancer Cell 2016;30:832–3.
47. Raschke WC, Baird S, Ralph P, Nakoinz I. Functional macrophage cell lines transformed by Abelson leukemia virus. Cell 1978;15:261–7.
48. Mareel M, Leroy A. Clinical, cellular, and molecular aspects of cancer invasion. Physiol Rev 2003;83:337–76.
49. Shapiro SD, Kobayashi DK, Ley TJ. Cloning and characterization of a unique elastolytic metalloproteinase produced by human alveolar macrophages. J Biol Chem 1993;268:23824–9.
50. Hofmann HS, Hansen G, Richter G, Taege C, Simm A, Silber RE, et al. Matrix metalloproteinase-12 expression correlates with local recurrence and metastatic disease in non-small cell lung cancer patients. Clin Cancer Res 2005;11:1086–92.
51. Ng KT, Qi X, Kong KL, Cheung BY, Lo CM, Poon RT, et al. Overexpression of matrix metalloproteinase-12 (MMP-12) correlates with poor prognosis of hepatocellular carcinoma. Eur J Cancer 2011;47:2299–305.
52. Kerkela E, Saarialho-Kere U. Matrix metalloproteinases in tumor progression: focus on basal and squamous cell skin cancer. Exp Dermatol 2003;12:109–25.
53. Wu D, Chen K, Bai Y, Zhu X, Chen Z, Wang C, et al. Screening of diagnostic markers for osteosarcoma. Mol Med Rep 2014;10:2415–20.